Modulation Schemes for Single-Laser 100 Gb/s Links: Multicarrier

Jose Krause Perin, Milad Sharif, and Joseph M. Kahn, *Fellow, IEEE*

Abstract—We evaluate multicarrier modulation methods for 100 Gb/s single-wavelength data center interconnects. We consider two different orthogonal frequency-division multiplexing (OFDM) techniques: DC-biased OFDM (DC-OFDM) and asymmetrically clipped optical OFDM (ACO-OFDM). We also consider two different techniques for bit loading and power allocation: fixed bit loading with preemphasis and optimized bit loading and power allocation. We first present a semianalytical performance and complexity evaluation of these OFDM methods including the effects of linear filtering, clipping, and quantization. We then include the effects of chromatic dispersion and chirp, as well as intensity and shot noises. Performance is quantified in terms of the required average optical power to achieve a target bit-error probability for a given modulator bandwidth. Complexity is quantified in terms of the resolution and sampling rate required of digital-to-analog (DAC) and analog-to-digital (ADC) converters, as well as the number of signal processing operations required. For each OFDM technique, we adjust the clipping ratio to minimize the optical power requirement. For DC-OFDM, taking into account the DAC frequency response reduces the optical power requirement up to 2 dB. ACO-OFDM is more power efficient and requires lower DAC/ADC resolution than DC-OFDM, but ACO-OFDM requires prohibitively high sampling rates owing to its poor spectral efficiency.

Index Terms—Asymmetrically clipped optical OFDM (ACO-OFDM), communications system performance and complexity, data center interconnects, DC-biased OFDM (DC-OFDM), direct detection, discrete multi-tone, intensity modulation, multi-carrier optical systems, orthogonal frequency-division multiplexing.

I. INTRODUCTION

SHORT-RANGE optical links, such as those in data centers, have achieved high bit rates in recent years using several independent lanes modulated by non-return-to-zero ON–OFF keying (NRZ-OOK). To minimize the number of lanes required at future bit rates of 400 Gb/s and 1.0 (or 1.6) Tb/s, it is desirable that each lane achieve a bit rate of 100 Gb/s per wavelength per single-mode fiber (SMF). These "single-laser 100G links" are intended to minimize optical component count, power consumption and size [1], and may facilitate optical switching in data center networks.

In single-laser 100G links, a modulation format compatible with direct detection and achieving a spectral efficiency higher than OOK [2] is needed, given the limited bandwidth of external modulators or directly modulated lasers (DMLs). Several schemes have been studied, including pulse-amplitude modulation (PAM) [3]–[5], carrierless amplitude-and-phase [5]–[8], quadrature amplitude modulation (QAM) [9], orthogonal multi-pulse modulation or orthogonal PAM [10], and orthogonal frequency-division multiplexing (OFDM) [5], [6]. OFDM, when combined with optimized bit loading and power allocation, is sometimes referred to as discrete multi-tone.

In this and in a companion paper [11], we present a comprehensive study of these modulation formats for single-laser 100G links. As a complement to prior simulation-based studies, we use analytical models to evaluate performance and complexity whenever possible, since analysis is more generally applicable and fosters insight into design optimization and the relative merits of the various schemes.

The companion paper [11] treats single-carrier modulation formats. This paper focuses on multicarrier formats, including DC-biased OFDM (DC-OFDM) [6] and asymmetrically clipped optical (ACO-OFDM) [12]. These formats differ in how they meet the non-negativity constraint of the intensity-modulated optical channel, and they achieve different tradeoffs between power efficiency and spectral efficiency.

Initially, we develop analytical models for performance and complexity considering modulation bandwidth constraints, thermal noise, clipping, and quantization, and neglecting other noise sources and chromatic dispersion (CD), assuming a single wavelength at the dispersion zero. We compare the performance of the various OFDM formats as a function of the modulation bandwidth and study tradeoffs between clipping and quantization noise. We compare the two OFDM formats in terms of the resolution and sampling rate required of digital-to-analog and analog-to-digital converters (DACs and ADCs) and the complexity of digital signal processing (DSP). DACs and ADCs are particularly critical, as they are likely to represent the single largest contribution to the power consumption of single-laser 100G links [6]. After this initial analysis, we select the most promising system designs and consider a system using coarse wavelength-division multiplexing (CWDM) to enable higher bit rates, where it is necessary to consider the effects of CD and modulation chirp. We also study the effects of shot noise and intensity noise.

The remainder of this paper is organized as follows. In Section II, we present a system model used in our analysis. In Section III, we review the various OFDM formats. In Section IV, we discuss major system impairments and how they affect system design and performance. In Section V, we study the performance penalty as a function of the modulation
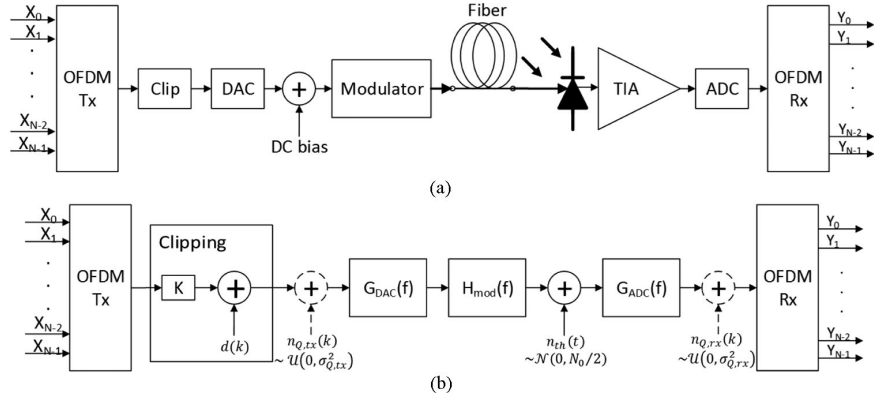
Fig. 1. (a) System block diagram, and (b) equivalent linear model.

bandwidth, considering both infinite and finite DAC/ADC resolution. In Section VI, we determine the required DAC/ADC resolution and sampling rate, as well as the number of DSP operations required for the various OFDM formats. In Section VII, we study the performance penalty from CD and the impact of shot and intensity noises. We present conclusions in Section VIII.

II. SYSTEM MODEL

The system model diagram is shown in Fig. 1(a). The discrete-time signal generated by the OFDM modem is clipped and converted to the analog domain, where an appropriate dc bias is added to make the signal non-negative. Assuming transmission near the zero-wavelength dispersion ($\sim$1310 nm for standard SMF), CD is negligible, and we can focus on the modulator and receiver, which are modeled as linear systems. As discussed in Section IV, non-linear distortions such as clipping and quantization can be represented by additive noises; clipping is modeled as an attenuation factor K and an uncorrelated noise $d(k)$, whereas quantization in the DAC and ADC is modeled by an additive uniform-distributed white noise. Thus, the system can be described by the equivalent linear model shown in Fig. 1(b).

We consider intensity modulation using DMLs or electro-absorption modulators (EAMs). DMLs are the simplest and most cost-effective solution, and have been demonstrated with bandwidths up to 34 GHz [13]. DMLs can be modeled by second-order linear systems, which follow directly from solving the laser rate equations. EAMs are available at much higher bandwidths, with research demonstrations up to 80 GHz [14]. In EAMs, the bandwidth-limiting factor is parasitic capacitance and inductance. EAMs are typically modeled as lumped-element circuits with two dominant poles [15], [16]. Hence, in this work, both DMLs and EAMs are modeled by a two-pole linear system $H_{\text{mod}}(f)$, whose cut-off frequency ($f_{3\text{dB}}$) is significantly less than the bit rate, and thus poses a significant bandwidth limitation.

The receiver, which includes the photodiode, transimpedance amplifier (TIA), and ADC, is characterized by a frequency response $G_{ADC}(f)$, since the anti-aliasing filter at the ADC has typically narrower passband and sharper transition band than the photodiode and the TIA.

Thermal noise is added by the TIA. TIAs have input-referred noise ($\bar{I}_{n,\text{in}}$) ranging from 14 up to $55.7\,\text{pA}/\sqrt{\text{Hz}}$, with bandwidths from 22 up to 70 GHz [17, Table 2]. $\bar{I}_{n,\text{in}}$ is easily related to the thermal noise double-sided power spectral density ($N_0/2$) by $N_0 = \bar{I}_{n,\text{in}}^2$. Initially, we consider thermal noise and quantization noise. The impact of shot and intensity noise is discussed in Section VII.

We model quantization in the DAC and ADC explicitly, since DAC/ADC resolution is likely to be a critical system design parameter for single-laser 100G links. The additive noise from quantization is indicated by dashed lines in Fig. 1(b), as it is absent when we consider the ideal case of infinite DAC/ADC resolution.

We assume a weak forward error-correction code such as RS (255, 239), which has a net coding gain of 5.6 dB at 10^{-12} bit-error ratio (BER), an input BER threshold of 1.8×10^{-4} to achieve 10^{-12} BER, and overhead of $\sim$7%. This code, and others with similar properties, are commonly used in transport networks [18], [19]. While stronger codes can provide higher gains, their complexity is prohibitive for single-laser 100G links. On the other hand, without coding, single-laser 100G links presumably cannot achieve the required 10^{-12} BER, and are difficult to analyze, since it is difficult to formulate system models that are accurate to such low BERs.

III. ORTHOGONAL FREQUENCY-DIVISION MULTIPLEXING

We consider two different OFDM techniques: DC-OFDM and ACO-OFDM, which differ in how they meet the non-negativity constraint of the intensity-modulated optical channel. In DC-OFDM, a relatively high dc bias is added to minimize clipping distortion. By contrast, in ACO-OFDM, the entire negative excursion of the signal is clipped, and clipping distortion is avoided by encoding information only on the odd subcarriers [12]. Signal spectra for the two techniques are shown in Fig. 2.

In the general OFDM transmitter shown Fig. 2, a discrete-time OFDM symbol is generated by performing an $N \cdot \text{IDFT}(\cdot)$ operation, yielding

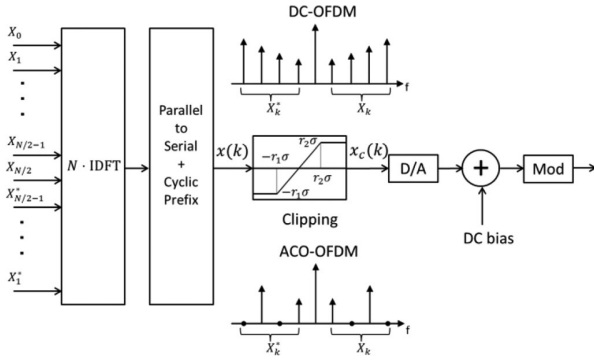$$\tilde{x}(k) = \sum_{n=0}^{N-1} X_n \exp\left(j\frac{2\pi}{N}nk\right), k = 0, \ldots, N-1, \quad (1)$$

Fig. 2.   Block diagram of the OFDM transmitter.

where the symbol transmitted at the nth subcarrier X_n is chosen from a M_n-QAM constellation with average power $P_n = E(|X_n|^2)$. M_n and P_n are determined, respectively, by bit loading and power allocation methods, as discussed in Section IV-A.

By the central limit theorem, for N sufficiently large, the OFDM signal is Gaussian-distributed, i.e., $\tilde{x}(k) \sim N(0, \sigma^2)$, where the variance or signal power is

$$\sigma^2 = E\left(|\tilde{x}(k)|^2\right) = 2 \sum_{n=1}^{N/2-1} P_n. \tag{2}$$

Note that $\tilde{x}(k)$ is real valued, since Hermitian symmetry is enforced, i.e., $X_n = X_{N-n}^*$. Moreover, for ACO-OFDM $X_n = 0$ for n even. Given a bit rate R_b, these conditions on X_n increase the OFDM symbol rate R_s, which is

$$R_s = 2p \frac{R_b}{\log_2 M}. \tag{3}$$

Here, M is the constellation size, assumed the same for all subcarriers, while $p = 1$ or 2 for DC-OFDM or ACO-OFDM, respectively accounts for the condition on the even subcarriers.

Due to oversampling and cyclic prefix (CP) insertion, the actual sampling rate (f_s) of the OFDM signal must be further increased to maintain the bit rate:

$$f_s = \frac{N + N_{CP}}{N} r_{os} R_s, \tag{4}$$

where N_{CP} is the CP length, and r_{os} is the oversampling ratio.

Note that $N_u = N/(pr_{os})$ subcarriers are effectively used to transmitted data, as oversampling is assumed implemented by zero-padding in the frequency domain.

After parallel-to-serial conversion and CP insertion, the discrete-time OFDM signal $x(k)$ is clipped at levels $-r_1\sigma$ and $r_2\sigma$ to reduce the required dynamic range of the DAC:

$$x_c(k) = \begin{cases} -r_1\sigma, & x(k) \leq -r_1\sigma \\ x(k), & -r_1\sigma < x(k) < r_2\sigma \\ r_2\sigma, & x(k) \geq r_2\sigma \end{cases}, \tag{5}$$

where $r_1 = r_2 = r$ for DC-OFDM; $r_1 = 0$, and $r_2 = r$ for ACO-OFDM. The factors r_1 and r_2 are referred to as clipping ratios. This definition allows us to easily calculate the clipping probability: $P_c = Q(r_1) + Q(r_2)$, where $Q(x)$ is the Q-function for the tail probability of a Gaussian distribution.

Note that a clipping event does not necessarily result in a bit error event.

The clipped signal is converted to the analog domain by the DAC and an appropriate dc bias is added to make the signal non-negative. Assuming that the ADC and the electrical-to-optical conversion have unit dc gain, the average optical power $\bar{P}$ equals the average electrical signal plus dc bias:

$$\bar{P} = \begin{cases} r\sigma, & \mathrm{DC-OFDM} \\ \dfrac{\sigma}{\sqrt{2\pi}}, & \mathrm{ACO-OFDM} \end{cases}, \tag{6}$$

where for ACO-OFDM, $\bar{P}$ follows directly from calculating the mean value of the clipped Gaussian distribution and assuming r large [12]. Equation (6) clearly indicates the average-power advantage of ACO-OFDM over DC-OFDM.

The dc bias required for DC-OFDM can be reduced by noticing that after the DAC, the signal variance is reduced, and therefore the full dc bias $r\sigma$ is not necessary to make the signal non-negative. Hence, we can add a smaller dc bias $r\sigma'$, where

$$\sigma'^2 = 2 \sum_{n=1}^{N/2-1} P_n |G_{DAC}(f)|^2 < \sigma, \tag{7}$$

where $G_{DAC}(f)$ is the frequency response of the DAC. Thus the average optical power becomes $\bar{P} = r\sigma'$. As shown in Section V, this strategy reduces the optical power penalty by up to 2 dB.

IV. SYSTEM IMPAIRMENTS

A. Non-Flat Channel Frequency Response

The non-flat frequency response of the channel causes some subcarriers to be attenuated more than others. Thus, to use all subcarriers effectively and ensure equal BER performance, we must perform power allocation, bit loading, or a combination of the two. We consider two alternatives: (i) constant bit loading and preemphasis (channel inversion), and (ii) optimized bit loading and power allocation.

In the preemphasis or channel inversion approach all subcarriers have the same constellation size M, but their power is inversely proportional to the channel gain at their corresponding frequencies: $P_n \propto |K G_{tot}(f_n)|^{-2}$, where $G_{tot}(f) = G_{DAC}(f) H_{\mathrm{mod}}(f) G_{ADC}(f)$ is simply the frequency response of the equivalent linear system shown in Fig. 1(b). Hence, at the receiver, all subcarriers have the same power, and signal-to-noise ratio (SNR), provided the noise is white.

In the optimized bit loading and power allocation method, the constellation size of each subcarrier is determined by solving the margin maximization problem [20]. In this optimization problem, we minimize the total power subject to a bit rate constraint. Formally,

$$\min_{P_n} P_t = 2 \sum_{n=1}^{N/2-1} P_n$$

$$\text{subject to } b = \sum_{n=1}^{N/2-1} \log_2\left(1 + \frac{P_n \mathrm{GNR}_n}{\Gamma}\right). \tag{8}$$

Here, Γ is referred to as the "gap to capacity," and represents the SNR penalty for using a suboptimal coding scheme instead of a capacity-achieving coding scheme. A gap of 0 dB means that the maximum bit rate of the channel can been achieved. GNR_n is defined as the channel gain-to-noise ratio at the nth subcarrier. Note that GNR_n is related to the SNR at the nth subcarrier by $SNR_n = P_n GNR_n$. The solution to the optimization problem in (8) minimizes the average optical power, since $\bar{P} \propto \sigma = \sqrt{P_t}$, as in (6).

The optimization problem (8) can be solved via Lagrange multipliers, resulting in the conventional water-filling solution. However, in practice, we employ the Levin-Campello (LC) algorithm [21] to obtain constellations with integer numbers of bits. Roughly speaking, this algorithm transfers bits from bad (more attenuated) subcarriers to good subcarriers, so that bad subcarriers can achieve the target BER at smaller SNRs, and thus requiring less power than in the preemphasis method. Implementation of the LC algorithm is described in [20]. This algorithm has two stages. In the first stage, an arbitrary bit distribution is made efficient. Efficiency in this context means that there is no movement of a bit from one subcarrier to another that can reduce the signal power. The next stage is the so-called B-tightening stage, where the number of bits in appropriate subcarriers is increased or reduced to ensure that the constraint in the bit rate is met. We have restricted the minimum constellation size to 4 (i.e., QPSK), to prevent the LC algorithm from excessively increasing the constellation size of good subcarriers by transferring all the bits from bad subcarriers to them.

B. Clipping Distortion

Clipping is necessary to reduce the dynamic range of the DAC and ADC. Even ignoring DAC/ADC limitations, clipping the negative tail is necessary to meet the non-negativity constraint of the intensity-modulated optical channel. Moreover, modulator nonlinearities may clip the positive tail as well.

Here, we extend the theory derived in [12] for ACO-OFDM to encompass both DC- and ACO-OFDM with two clipping levels. Assuming $x(k) \sim N(0, \sigma^2)$, we can apply Bussgang's Theorem [22], and (5) can be written as

$$x_c(k) = Kx(k) + d(k), \qquad (9)$$

where $d(k)$ is a random process that is uncorrelated with $x(k)$, i.e., $E(d(k)x^*(k)) = 0$. Here, K is a constant that depends only on the nonlinear amplitude distortion [22], which is clipping in this case. It can be shown that

$$K = 1 - Q(r_1) - Q(r_2). \qquad (10)$$

Note that for $r_1 = 0$ and $r_2 \to \infty$ (i.e., ACO-OFDM with clipping only at the zero level), $K = 1/2$, as previously shown in [12]. For ACO-OFDM, it can be further shown that $d(k)$ only has frequency components on the even subcarriers, which intentionally do not carry data [12].

For DC-OFDM, $d(k)$ does cause distortion on the data-bearing subcarriers. The power in $d(k)$, ignoring its dc level, is given by

$$\mathrm{Var}(d(k)) = \mathrm{Var}(x_c(k)) - K^2\sigma^2, \qquad (11)$$

where $\mathrm{Var}(x_c(k))$ is a function of r_1, r_2 and σ^2, which can be obtained from the distribution of $x_c(k)$, i.e., a Gaussian distribution clipped at $-r_1\sigma$ and $r_2\sigma$.

C. Quantization

We assume the same effective number of bits (ENOB) for both DAC and ADC. At very high sampling rates (currently above about 30 GS/s), there is no significant difference in the effective resolution of DACs and ADCs; both are currently limited to about 6 bits [23], [24]. Moreover, noise-like OFDM waveforms require relatively high resolution from both DAC and ADC.

Quantization noise is generally modeled as an additive, uniformly distributed white noise, whose variance is given by

$$\sigma_{Q,\{\cdot\}}^2 = (1 - P_c)\frac{\Delta X_{\{\cdot\}}}{12 \cdot 2^{2\mathrm{ENOB}}}, \qquad (12)$$

where $\sigma_{Q,tx}^2$ and $\sigma_{Q,rx}^2$ denote the quantization noise variance at transmitter and receiver, respectively. Similarly, $\Delta X_{\{\cdot\}}$ denotes the dynamic range of the quantizer at the transmitter or receiver. Note that the clipping probability reduces the quantization noise variance, since at the clipped levels there is no error due to quantization, provided they are also quantization levels.

The dynamic range of the quantizer depends on the input signal statistics. At the transmitter, the input signal is the clipped OFDM signal $x_c(k)$. Therefore, the quantization noise variance at the transmitter is given by

$$\sigma_{Q,tx}^2 = \begin{cases} (1 - P_c)\dfrac{r_{tx}^2\sigma^2}{3 \cdot 2^{2\mathrm{ENOB}}}, & \mathrm{DC - OFDM} \\[3mm] (1 - P_c)\dfrac{r_{tx}^2\sigma^2}{12 \cdot 2^{2\mathrm{ENOB}}}, & \mathrm{ACO - OFDM}. \end{cases} \qquad (13)$$

For a given transmitter clipping ratio r_{tx}, the signal excursion of DC-OFDM is twice the signal excursion of ACO-OFDM. As a result, quantization noise variance for DC-OFDM is four times greater. Moreover, assuming negligible clipping distortion at data-bearing subcarriers, we have $P_c \approx 0$ for DC-OFDM, and $P_c \approx 1/2$ for ACO-OFDM, which further reduces the quantization noise in ACO-OFDM.

At the receiver, the signal has undergone linear filtering. A DC-OFDM signal can still be considered Gaussian-distributed with variance reduced by the channel frequency response:

$$\sigma_{rx}^2 = 2 \sum_{n=1}^{N/2-1} P_n |G_{tot}(f_n)|^2. \qquad (14)$$

Thus, the dynamic range of the quantization for DC-OFDM at the receiver is given by $\Delta X_{rx} = 2r_{rx}\sigma_{rx}$, where r_{rx} is the clipping ratio at the receiver.

ACO-OFDM, on the other hand, is highly asymmetric. As an approximation, we can consider the received ACO-OFDM signal as non-negative with mean $\sigma/\sqrt{2\pi}$ (assuming all filters have unit dc gain), with the positive tail approximated by a Gaussian of variance σ_{rx}^2. For ACO-OFDM the sum in (14) is over the odd subcarriers only. Thus the dynamic range of the quantizer for ACO-OFDM at the receiver is given by $\Delta X_{rx} = \sigma/\sqrt{2\pi} + r_{rx}\sigma_{rx}$. This approximation is not ultimately important, as we optimize the clipping ratio both at the
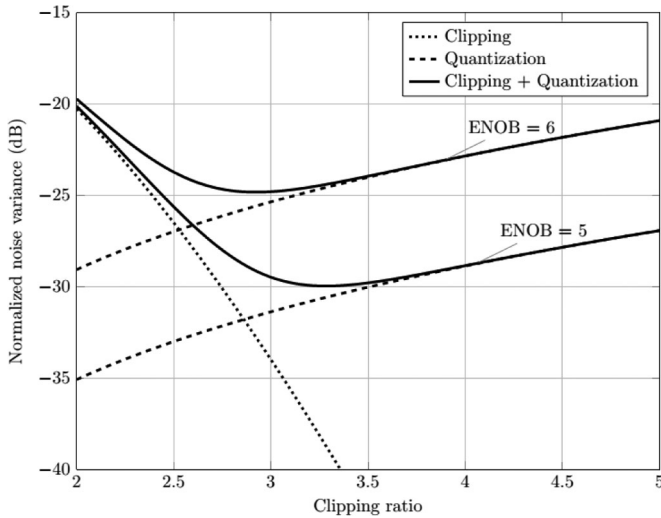
Fig. 3. Normalized clipping and quantization noise variance as a function of clipping ratio for DC-OFDM.

transmitter and at the receiver to minimize the power penalty. It is just a convenient way to express the clipping and quantization levels in terms of the signal power. This facilitates the analysis of clipping and quantization noises, as well as the required ENOB.

Hence, the quantization noise variance at the receiver is given by

$$
\sigma_{Q,rx}^2 =
\begin{cases}
\dfrac{r_{rx}^2 \sigma_{rx}^2}{3 \cdot 2^{2\text{ENOB}}}, & \text{DC} - \text{OFDM} \\[4mm]
\dfrac{\left(\dfrac{\sigma}{\sqrt{2\pi}} + r_{rx}\sigma_{rx} \right)^2}{12 \cdot 2^{2\text{ENOB}}}, & \text{ACO} - \text{OFDM},
\end{cases}
\tag{15}
$$

Fig. 3 shows clipping and quantization noise variances normalized by the signal power as a function of the clipping ratio for DC-OFDM. We focus on DC-OFDM, since the clipping ratio directly affects the required dc bias and consequently the overall power penalty.

There is a clear tradeoff between clipping and quantization noises. Although the minimum total noise is achieved around $r = 2.8$ for ENOB = 5, and $r = 3.8$ for ENOB = 6, we must choose the clipping ratio so as to make clipping noise negligible compared to quantization noise. This is because clipping noise has several undesired characteristics, such as non-white power spectrum and heavy tails, whereas quantization noise can be accurately modeled as a bounded uniform white noise. Indeed, the optimization performed over the clipping ratios to minimize the optical power penalty in Sections V and VI-A yields clipping ratios in the range of 3.7 to 4.5, where clipping noise becomes negligible, as can be seen in Fig. 3.

D. Non-Ideal Extinction Ratio

A non-ideal transmitter extinction ratio r_{ex}, which is defined as the ratio the between minimum and the maximum optical powers, gives rise to an optical power penalty $\Delta \bar{P}_{ex}$ As an example, for DC-OFDM, this penalty is given by a simple

equation:

$$
\Delta \bar{P}_{ex} = \frac{1 + r_{ex}}{1 - r_{ex}}
\tag{16}
$$

Typically, r_{ex} lies between -20 and -10 dB, which results in a small penalty between 0.09 and 0.85 dB, respectively. For this reason we disregard the non-ideal extinction ratio penalty in the analytical development in Section V, but we include it in the numerical results of Section VII.

V. PERFORMANCE EVALUATION: NEGLIGIBLE CD

In this section, we evaluate the performance of DC- and ACO-OFDM assuming the equivalent linear system discussed in Section II and depicted in Fig. 1(b). We evaluate the relationship between the cutoff frequency of the modulator and the optical power to achieve the target BER of 1.8×10^{-4}. This analysis highlights the advantages and disadvantages of DC- and ACO-OFDM, as well as the benefits of using fixed bit loading and preemphasis or optimized bit loading and power allocation.

To make our results independent of the actual thermal noise power spectral density of the TIA, we normalize the required average optical power by the average optical power required by an NRZ-OOK system to achieve the same BER at the same bit rate, operating on an ideal AWGN intensity-modulated direct-detected (IM-DD) optical channel. This is motivated by the fact that NRZ-OOK is the format traditionally used in optical communications, and the required optical power in such AWGN channel is given by the simple expression

$$
\bar{P}_{OOK,req} = \frac{1}{R} \sqrt{\frac{R_b N_0}{2}} Q^{-1} \left(\text{BER}_{req} \right),
\tag{17}
$$

where R is the photodiode responsivity, and R_b is the bit rate, which, as discussed in Section II, is set to $R_b = 107$ GHz. Equations for the BER of DC- and ACO-OFDM on an ideal AWGN IM-DD optical channel are presented in appendix.

The maximum average optical power is limited in about 9.4 dBm due to eye-safety restrictions (IEC 60825-1). Thus, as an example, power penalties up to 14 dB with respect to NRZ-OOK are still within the power budget, assuming CWDM transmission of four channels, with link attenuation of up to 5 dB and $\bar{P}_{OOK,req} \approx -16.1\,\text{dBm}$, which corresponds to $\bar{I}_{n,in} = 30\,\text{pA}/\sqrt{\text{Hz}}$, and $\text{BER}_{req} = 1.8 \times 10^{-4}$.

A. Infinite DAC/ADC Resolution

The SNR on each subcarrier at the receiver assuming infinite resolution DAC/ADC is given by

$$
\text{SNR}_n = \frac{2K^2 N \left| G_{DAC}\left(f_n\right) H_{\text{mod}}\left(f_n\right) \right|^2 P_n}{N_0 f_s},
\tag{18}
$$

where for ACO-OFDM this expression is only valid for n odd; assuming negligible clipping distortions on the data-bearing subcarriers we have $K \approx 1$ for DC-OFDM, and $K \approx 1/2$ for ACO-OFDM. The sampling rate f_s is given by (4) with the CP length chosen to accommodate the duration of the channel impulse response. The required sampling rate and OFDM signal bandwidth are discussed further in the complexity

TABLE I
SAMPLING RATE AND OFDM SIGNAL BANDWIDTH FOR $R_b = 107$ GB/S

Constellation	DC-OFDM	ACO-OFDM
16-QAM	65.8 GS/s	131.6 GS/s
	26.7 GHz	53.4 GHz
64-QAM	43.9 GS/s	87.7 GS/s
	17.83 GHz	35.6 GHz

analysis in Section VI-B and summarized in Table I. Note that the $G_{ADC}(f_n)$ does not appear in (18), as it affects both the noise and signal equally. However, (18) is valid only when aliasing is negligile.

In this section, for simplicity, we omit scaling factors such as the modulator electro-optical conversion gain and the photodiode responsivity, which can be incorporated by changing the gains of the appropriate frequency responses.

Although SNR_n is directly proportional to N, in practice, it may be desirable to minimize the number of subcarriers employed for various reasons. For example, it is well known that the peak-to-average power ratio increases in proportion to N, which increases clipping distortion. Furthermore, the number of real operations in the DSP of OFDM systems increases with $N \cdot \log_2 N$, as discussed in Section VI-C.

For fixed bit loading and preemphasis, the target BER direclty implies a required SNR_n, since all the subcarriers have the same constellation size (e.g., $\text{SNR}_n = 17.85$ dB, for 16-QAM; $\text{SNR}_n = 23.91$ dB, for 64-QAM at a target BER of 1.8×10^{-4}). Hence, P_n follows direclty by solving (18).

For the optimized bit loading and power allocation, we must first calculate GNR_n and the gap Γ to achieve the target BER, e.g., assuming square constellations, for $\text{BER} = 1.8 \times 10^{-4}$, $\Gamma \approx 6.3$ dB. The LC algorithm gives us the optimized bit loading $b_n = \log_2 M_n$ and the power allocation P_n that minimizes the total power P_t.

The optical power penalty is obtained by normalizing the required average optical power $\bar{P}_{req}$, calculated from (6), by $\bar{P}_{OOK,req}$ given by (17). For DC-OFDM, we also consider the proposed reduced dc bias taking into account the DAC frequency response as in (7).

The procedure described to calculate the optical power $\bar{P}_{req}$ disregards clipping noise. Thus, r is set to the minimum value at each the target BER can still be achieved. This ensures small clipping distortion, without excessively increasing the dc bias and consequently the optical power penalty. This yields r in the range of 3.7 to 4.2 for 16-QAM and 3.9 to 4.5 for 64-QAM.

Fig. 4 shows the optical power penalty for DC- and ACO-OFDM with (a) 16-QAM and (b) 64-QAM for $N = 64$, assuming $r_{os} = 1.23$. $N = 64$ is high enough to make the CP penalty negligible without excessively increasing the number of DSP operations per bit, which increases logarithmically with N, as shown in (23). Note, however, that as shown in appendix, for an ideal unipolar AWGN channel, the power penalty does not depend on the number of subcarriers. $H_{\text{mod}}(f)$ is a second-order system with unit damping ratio. DA conversion is modeled by a zero-order hold followed by a fifth-order Bessel filter with

cut-off frequency equal to the OFDM bandwidth, which is given by $f_s/(2r_{os})$ and summarized in Table I. The antialiasing filter $G_{ADC}(f)$ is modeled as a fourth-order Gaussian filter with cut-off frequency also equal to the OFDM signal bandwidth. The use of these non-ideal interpolation and antialiasing filters typically requires $r_{os} > 1.2$. An input-referred noise level $\bar{I}_{n,\text{in}} = 30\,\text{pA}/\sqrt{\text{Hz}}$ is assumed, corresponding to an intermediate value among TIAs presented in the literature [17].

The dotted lines in Fig. 4(a) and (b) indicate the power penalty for DC- and ACO-OFDM on an ideal AWGN IM-DD optical channel calculated according to (28). Note that there is an inherent 2-dB penalty in going from 16-QAM to 64-QAM. The difference between the penalties on the actual channel (solid lines) and the ideal channel (dotted lines) is caused primarily by the dc bias added to make the signal non-negative after DA conversion and by the power allocation for the non-flat channel frequency response, and secondarily by the CP penalty.

For DC-OFDM, the dc bias is the major factor responsible for the optical power penalty. This is indicated by the relatively small gap between the solid and dotted lines in Fig. 4(a) and (b). By taking into account the frequency response of the DAC as discussed in Section III, we can reduce the required dc bias, and consequently the power penalty by up to 2 dB, as seen by the difference between the set of curves indicated by $r\sigma$ and $r\sigma'$ DC-OFDM in Fig. 4(a) and (b). Moreover, as expected, the gain obtained by using the optimized power allocation is significantly reduced as the cutoff frequency increases.

ACO-OFDM has a penalty of about 2.5 dB with respect to the dotted lines in Fig. 4(a) and (b) even when the cutoff frequency is high, due to the dc bias required after DA conversion. The continuous-time ACO-OFDM signal has a negative excursion because the impulse response of the DA filter has a negative excursion, which is small for Bessel filters. As the cutoff frequency is reduced, the penalty increases significantly, due to the high signal bandwidth of ACO-OFDM. This is mitigated through optimized power allocation, which provides gains of almost 3 dB. 64-QAM, shown in Fig. 4(b), also provides some improvement, especially at cutoff frequencies below 30 GHz, since it halves the signal bandwidth.

The results in Fig. 4 show that optimized bit loading and power allocation may reduce the power penalty when the modulator cutoff frequency is smaller than the signal bandwidth. The penalty reduction is largest for ACO-OFDM, which has poorer spectral efficiency compared to DC-OFDM. The power penalty reduction comes at the expense of using higher-order QAM constellations (up to 256-QAM). In the titles of Fig. 4, 16-QAM and 64-QAM refer to the nominal constellation size, i.e., the constellation size that results in the symbol rate given in (3).

B. Finite DAC/ADC Resolution

We now include quantization noise as calculated in Section IV-C.

Although quantization noise is uniformly distributed in the time domain, after the DFT at the receiver, the noise on each subcarrier becomes approximately Gaussian distributed, due to the Central Limit Theorem. Moreover, assuming the noises are
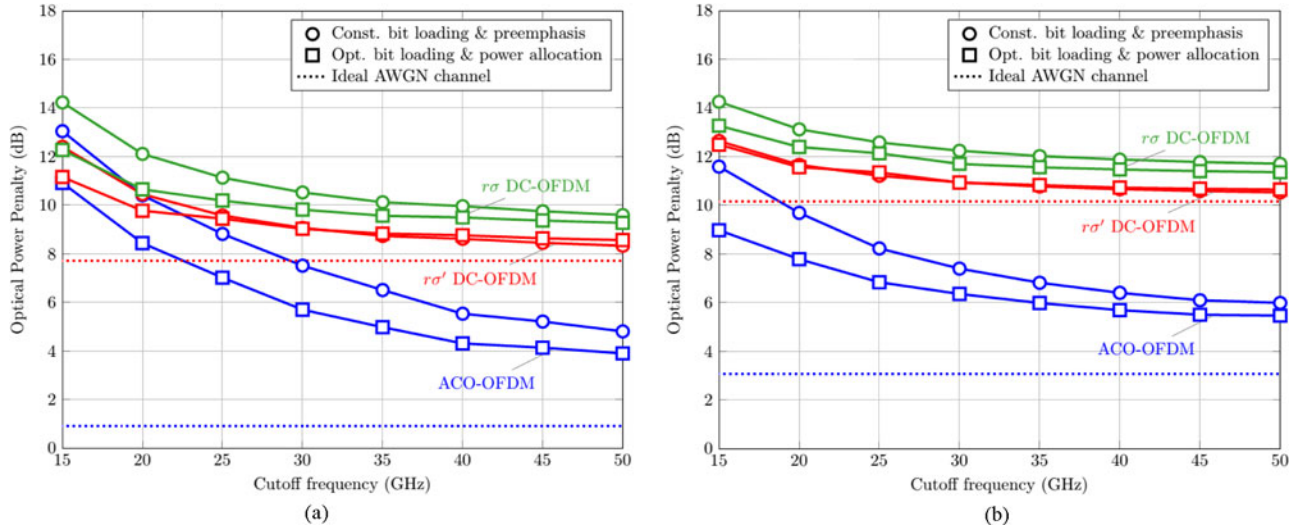
Fig. 4. Optical power penalty versus modulator cutoff frequency for (a) 16-QAM and (b) 64-QAM nominal constellation sizes. Dotted lines are the optical power penalties assuming an ideal AWGN optical channel, as computed in appendix. For DC-OFDM, red lines with caption $r\sigma$ DC-OFDM use the OFDM signal variance given by (2), and green lines with caption $r\sigma'$ DC-OFDM use the OFDM variance (7).
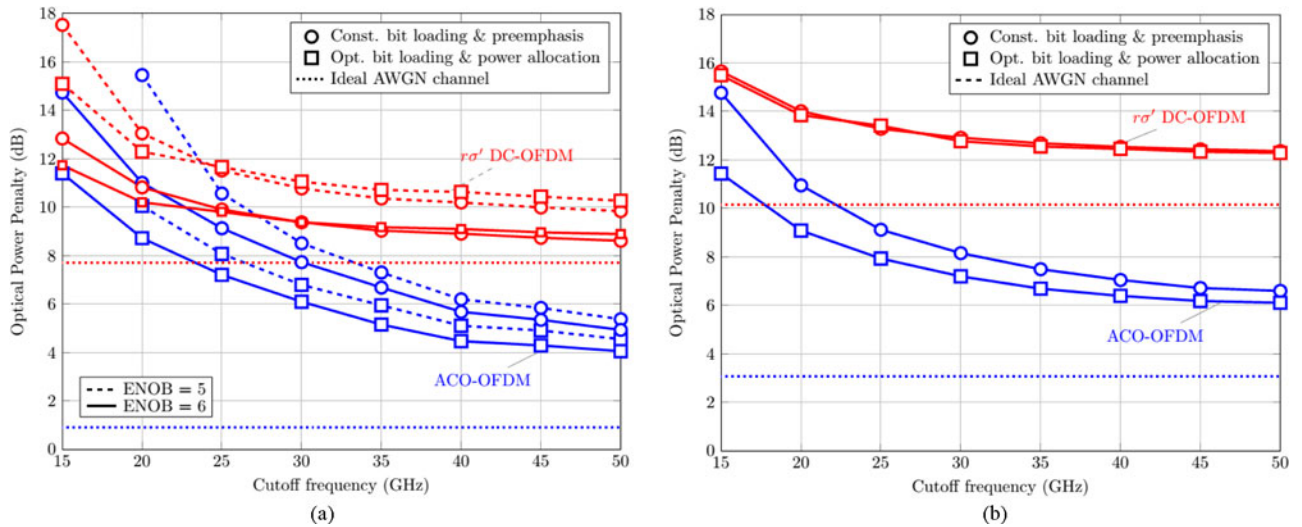

Fig. 5. Optical power penalty versus modulator cutoff frequency for (a) 16-QAM and (b) 64-QAM nominal constellation sizes. Dotted lines are the optical power penalties assuming an ideal AWGN channel, as computed in appendix. For 16-QAM, optical power penalties are shown for both ENOB = 5 (dashed lines) and ENOB = 6 (solid lines). For 64-QAM, it is only possible to use ENOB = 6.

uncorrelated, their variances add. Therefore, the SNR on the *n*th subcarrier is given by

$$\mathrm{SNR}_n = \frac{K^2 N |G_{tot}(f_n)|^2 P_n}{\frac{N_0}{2} f_s |G_{ADC}(f_n)|^2 + \sigma_{Q,tx}^2 |G_{tot}(f_n)|^2 + \sigma_{Q,rx}^2}.$$

(19)

To obtain the required optical power, (19) must be solved iteratively, as the quantization noise variances depend on P_n. Thus, we initially assume no quantization, and obtain a first estimate of the power $P_n^{(1)}$, which corresponds to the solution in the previous section. Using this value we calculate the quantization noise variances according to (13) and (15), and obtain a new estimate $P_n^{(2)}$ either through preemphasis (i.e., solving

(19) for P_n) or optimized power allocation (i.e., through the LC algorithm with $\mathrm{GNR}_n = \mathrm{SNR}_n / P_n$, where SNR_n is given by (19)). We repeat this procedure until the power converges to a final value $P_n^{(L)}$ after L iterations. Convergence may not occur if the required SNR is above the SNR ceiling due to quantization

Fig. 5 shows the power penalty including quantization for both 16- and 64-QAM. The simulation parameters are the same as used in the previous section. For clarity, we only show the results of DC-OFDM with reduced dc bias, as calculated in (7).

As expected, quantization induces an additional penalty. As suggested by (13) and (15), the penalty for quantization is smaller for ACO-OFDM than for DC-OFDM. Moreover, we note that for ACO-OFDM and 16-QAM DC-OFDM, there is virtually no difference between the penalty curves for ENOB

= 6 in Fig. 5, and the curves for infinite DAC/ADC resolution shown in Fig. 4. This indicates that ENOB = 6 is sufficient to obtain nearly optimal performance. However, for 64-QAM DC-OFDM with ENOB = 6 there is a 2-dB penalty with respect to infinite ADC/DAC resolution. This 2-dB penalty with respect to infinite ADC/DAC resolution is also observed for ACO-OFDM and 16-QAM DC-OFDM with ENOB = 5.

We only show curves of ENOB = 6 in Fig. 5(b) because the required SNR for 64-QAM (nominal constellation size) is above the SNR ceiling imposed by quantization, as further discussed in Section VI-A.

Similarly to the previous section, we see that optimized bit loading with power allocation provides some reduction of the optical power penalty for ACO-OFDM, but has little effect for DC-OFDM.

VI. COMPLEXITY ANALYSIS

We discuss the complexity of DC- and ACO-OFDM in terms of DAC/ADC sampling rate and resolution, and number of DSP operations. Unlike power consumption, these results do not depend on implementation choices and/or technology used.

A. DAC/ADC Resolution

Assuming the modulator cutoff frequency is approximately equal to the signal bandwidth, so that all subcarriers have the same power and bit loading, and considering the limit when quantization noise becomes dominant, equation (19) reduces to

$$\text{SNR}_n = \frac{K^2 N P_n}{\sigma_{Q,tx}^2 + \sigma_{Q,rx}^2}, \tag{20}$$

where $\sigma_{Q,tx}^2$ and $\sigma_{Q,rx}^2$ are given by (13) and (15), respectively. Note that $\sigma_{Q,tx}^2$ and $\sigma_{Q,rx}^2$ are proportional to the signal power σ^2, and that in the case of equal bit loading and power allocation we have $\sigma^2 = N_u P_n$. Thus, SNR_n has a ceiling in the quantization-noise limited regime.

We can solve (20) for the ENOB as a function of SNR_{req} that leads to the target BER:

$\text{ENOB}_{req} =$

$$\begin{cases} \frac{1}{2}\log_2\left(\frac{2r^2}{3r_{os}}\text{SNR}_{req}\right), & \text{DC} - \text{OFDM} \\ \frac{1}{2}\log_2\left(\frac{r^2 + 2\left(1/\sqrt{2\pi} + r\right)^2}{12r_{os}}\text{SNR}_{req}\right), & \text{ACO} - \text{OFDM}. \end{cases}$$
$$\tag{21}$$

This value of ENOB is actually a lower bound, as we have neglected thermal noise and filtering; however, it is useful to provide a first estimate of the required resolution for DC- and ACO-OFDM, allowing SNR_{req} to be calculated based on the target BER and the nominal constellation size of the OFDM signal.

Fig. 6 shows the required ENOB for DC- and ACO-OFDM with 16-QAM and 64-QAM constellation as a function of the clipping ratio for $r_{os} = 1.23$.
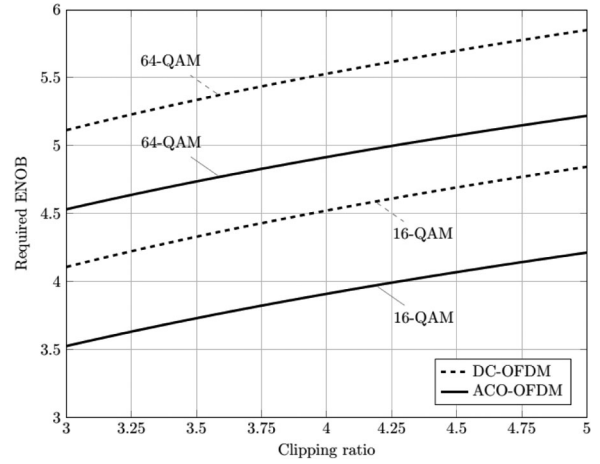

Fig. 6. Required ENOB to achieve target BER of 1.8×10^{-4} for DC-OFDM (dashed lines) and ACO-OFDM (solid lines) with 16- and 64-QAM nominal constellation sizes. The oversampling ratio is 1.23.

ACO-OFDM requires fewer bits since the signal excursion is half of the DC-OFDM. However, the difference does not go up to 1 bit as might be expected, because with ACO-OFDM, clipping reduces the signal power by 1/4, since $K = 1/2$.

This result shows that ENOB must be at least 5 for 16-QAM, and at least 6 for 64-QAM, considering only integer ENOB values. This result agrees well with the rule of thumb $\text{ENOB}_{req} \approx \log_2(\sqrt{M}) + 3$ for the resolution required of ADC to detect filtered single-carrier QAM signals [25].

B. DAC/ADC Sampling Rate

Given the short duration of the impulse response of the channel, N_{CP} is small compared to the number of subcarriers. In fact, N_{CP} does not exceed eight samples in the simulations performed in Section V. Thus, (4) can be approximated by

$$f_s = \frac{N + N_{CP}}{N} r_{os} R_s \approx r_{os} R_s. \tag{22}$$

Table I shows the sampling rate and signal bandwidth for DC- and ACO-OFDM with 16-QAM and 64-QAM. Note that the spectral efficiency of ACO-OFDM is half of the spectral efficiency of DC-OFDM, since half the subcarriers are not modulated in order to avoid clipping distortion. Consequently, the sampling rates for ACO-OFDM are prohibitively high. By contrast, DC-OFDM requires sampling rates that can be achieved by modern high-speed DAC/ADC [23].

C. DSP Complexity

The major DSP complexity in OFDM systems lies in calculation of the IDFT at the transmitter and the DFT at the receiver. These operations are performed effectively using a fast Fourier transform (FFT) algorithm. Assuming the split-radix algorithm, an FFT requires approximately $4 \cdot N \cdot \log_2 N$ real operations (multiplications and additions), where N is the FFT size. Specifically, the approximate number of additions is $8/3 \cdot N \cdot \log_2 N$ and the approximate number of multiplications is $4/3 \cdot N \cdot \log_2 N$ [26]. Therefore, the number of

real operations required per second at the transmitter is $4 \cdot N \cdot \log_2 N / T_{OFDM}$, where $T_{OFDM} = (N + N_{CP})/f_s$ is the OFDM symbol period. Thus, the transmitter requires $8 \cdot p \cdot r_{os} \cdot R_b \cdot \log_2 N / \log_2 M$ real operations per second.

For the OFDM receiver, we must also account for the complex single-tap equalizer on each data-bearing subcarrier, which corresponds to additional N_u complex operations. We neglect computations required to perform power allocation at the transmitter, as we assume that the power allocation is computed once and remains fixed.

The overall number of real operations per bit at the transmitter and at the receiver is

$$O_{TX} = 8pr_{os} \frac{\log_2 N}{\log_2 M}$$

$$O_{RX} = 4 \frac{2pr_{os}\log_2 N + 3}{\log_2 M}, \tag{23}$$

where, as defined previously, $p = 1$ for DC-OFDM and $p = 2$ for ACO-OFDM. Thus for given values of N, M, and r_{os}, ACO-OFDM requires twice as many real operations per bit as DC-OFDM. This is because ACO-OFDM requires roughly twice the sampling rate of DC-OFDM, so that DSP operations must be performed twice as fast.

VII. PERFORMANCE EVALUATION: NON-NEGLIGIBLE CD, SHOT AND INTENSITY NOISES

Sections V and VII showed that although ACO-OFDM has smaller power penalties, it requires prohibitively high sampling rate and DSP complexity, compared to DC-OFDM. Hence, we focus on DC-OFDM, and evaluate the effects of CD and chirp, as well as intensity and shot noises.

When using CWDM to enable 400 Gb/s or higher bit rates, some of the channels might experience non-negligible CD. The amount of dispersion depends on the number of channels as well as the channel spacing. Typically the channel spacing is 4.5 nm (LAN WDM) or 20 nm (CWDM). Although the former spacing can minimize dispersion, it may require temperature-controlled lasers, increasing cost and power consumption.

Both DMLs and EAMs exhibit chirp, i.e., instantaneous variation of the optical carrier frequency upon intensity modulation. The combined effects of CD and chirp cause phase-to-intensity conversion, which distorts the detected intensity signal. DMLs have both adiabatic and transient chirp, but the latter becomes dominant under high-frequency modulation [27]. EAMs exhibit transient chirp, which arises from the relationship between real and imaginary refractive indices dictated by causality [28]. Thus, for both DML and EAM, the phase modulation $\Delta\Phi(t)$ caused by intensity modulation is assumed to be described by

$$\Delta\Phi(t) \approx \frac{\alpha}{2}\ln(P(t)), \tag{24}$$

where α is the chirp parameter. In DMLs, α is also referred to as the linewidth enhancement factor, and is positive. In EAMs, α is typically smaller and may be positive or negative.
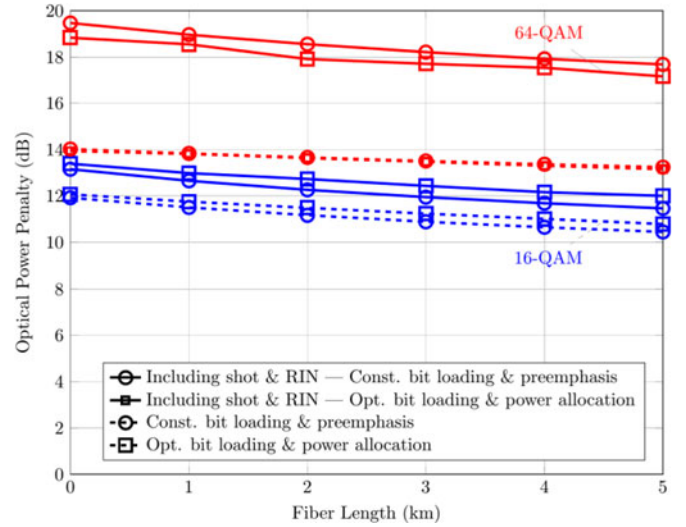

Fig. 7. Optical power penalty as a function of fiber length for DC-OFDM with 16- and 64-QAM nominal constellation sizes. Results assume $f_{3\,\mathrm{dB}} = 30\,\mathrm{GHz}$, $\bar{I}_{n,\mathrm{in}}^2 = 30\,\mathrm{pA}/\sqrt{\mathrm{Hz}}$, RIN $= -150\,\mathrm{dB/Hz}$, $\alpha = 2$, $r_{os} = 1.23$, $r_{ex} = -10\,\mathrm{dB}$, N $= 64$; $\lambda = 1250\,\mathrm{nm}$, implying $D \approx -6\,\mathrm{ps/nm/km}$ in SSMF and ENOB $= 5$ and 6 for 16-QAM and 64-QAM, respectively.

When transient chirp is dominant, the small-signal frequency response of the intensity channel is given by

$$H_{fib}(f, z) = \cos\theta - \alpha\sin\theta, \tag{25}$$

where z is the fiber length, $\theta = -0.5\beta_2(2\pi f)^2 z$ [29], and $\beta_2 = -(\lambda^2/2\pi c)D$, where D is the dispersion parameter. Note that for θ small, if $D\alpha > 0$, the second term in (25) is positive and hence reduces the fiber frequency response. Conversely, if $D\alpha < 0$, the second term becomes positive, which causes the fiber frequency response to increase, i.e., dispersion provides some gain. Naturally, the second case is preferable, as the fiber frequency response compensates for the modulator bandwidth limitations and consequently reduces the power penalty. For this reason, if $\alpha > 0$, we should use wavelengths shorter than the zero-dispersion wavelength so that $D < 0$.

We can use (25) to calculate the total frequency response of the channel and use this result for the aforementioned power allocation and preemphasis algorithms. Nonetheless, the system cannot be approximated well by the linear filtering system showed in Fig. 1(b), since CD is a linear operation only in terms of the electric field.

Fig. 7 shows the power penalty as a function of the fiber length. Due to the gain provided by the fiber frequency response, the power penalty decreases as the fiber length increases. Therefore, CD and chirp can be beneficial up to a certain span length. However, the distortion caused by the phase-to-intensity conversion causes an additional penalty as the fiber length increases. Hence, we must increase the power on the subcarriers in order to overcome this additional penalty.

This power allocation could be done by using the model proposed in [30], which has polynomial-time complexity, to calculate the distortion on each subcarrier and change its power and/or bit loading accordingly. Fortunately, for 100 Gb/s links
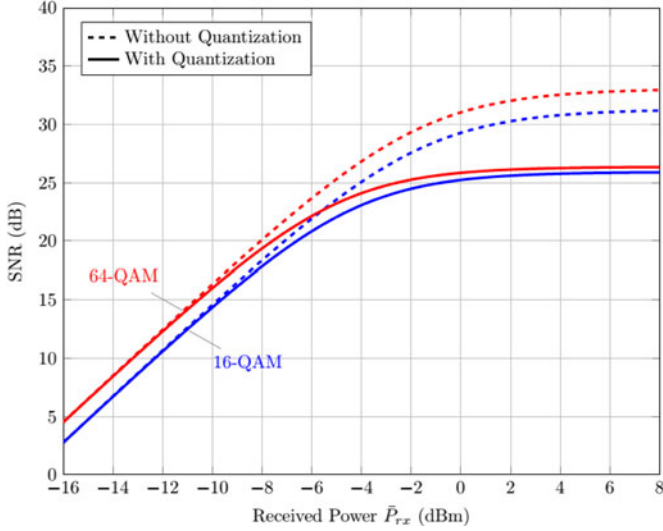
Fig. 8. SNR as a function of the received power including with (solid lines) and without (dashed lines) quantization noise. These curves were obtained for $\bar{I}_{n,\text{in}}^2 = 30\,\text{pA}/\sqrt{\text{Hz}}$, RIN $= -150\,\text{dB/Hz}$, $r_{os} = 1.23$, ENOB $= 6$, and $f_s = R_s$ as given in (3).

over the distances of interest for data centers (up to about 5 km), the phase-to-intensity distortion can be neglected. Fig. 7 also shows that there is little improvement by using optimized power allocation and bit loading rather than simply using preemphasis without bit loading. In fact, the curves overlap for 64-QAM.

Including shot noise and thermal noise has little effect on 16-QAM, but they increase the penalty by about 2 dB for 64-QAM. To evaluate the relative impact of the different noises, we can analytically calculate the SNR as a function of the received average optical power $\bar{P}_{rx}$ by disregarding bandwidth limitations in the channel and assuming that all noise sources are white over the bandwidth of interest:

$$\text{SNR} = \frac{r_{os}\left(\dfrac{R\bar{P}_{rx}}{r}\right)^2}{f_s\left(\dfrac{N_0}{2} + qR\bar{P}_{rx} + \text{RIN}\cdot R^2\bar{P}_{rx}^2\right) + 2\sigma_Q^2}, \quad (26)$$

where q is the electron charge, R is the photodiode responsivity, RIN is the relative intensity noise in linear units, and σ_Q^2 is the quantization noise variance, which is assumed to be the same at both transmitter and receiver and given by (13). All noises are assumed to be mutually uncorrelated, and after the IDFT they become approximately Gaussian-distributed. Thus, their variances add. In the denominator of (26), the three terms denote the thermal, shot, and intensity noise respectively. Note that the thermal noise variance is independent of the average optical power, while the shot and intensity noise variances have linear and quadratic dependencies on the average power, respectively.

Fig. 8 shows the SNR as a function of the received power $\bar{P}_{rx}$ for 16- and 64-QAM DC-OFDM. Curves for infinite and finite (ENOB $= 6$) DAC/ADC resolution are shown. For infinite DAC/ADC resolution, in the thermal-noise limited regime, the SNR increases linearly with the received power. After a certain threshold the SNR increases sub-linearly with $\bar{P}_{rx}$, until it

reaches a ceiling in the intensity-noise limited regime. When quantization noise is included, the SNR ceiling is smaller and is reached at lower power than in the intensity-noise limited regime. This indicates that quantization noise is the limiting noise for the performance of OFDM signals. Thus, intensity noise and shot noise do not cause significant additional penalties over those described in Section V.

VIII. CONCLUSION AND FUTURE WORK

We have evaluated the performance and complexity of two different OFDM formats for data center interconnects: DC-OFMD and ACO-OFDM.

The performance of these OFDM techniques was evaluated in terms of the optical power penalty with respect to the NRZ-OOK operating at the same bit rate on an ideal AWGN channel. The complexity of these OFDM techniques was measured in terms of the required DAC/ADC resolution, sampling rate, and the number of DSP operations.

As expected, there is a clear tradeoff between power and spectral efficiencies. ACO-OFDM is power efficient, as it allows clipping the signal at zero level. However, to avoid clipping distortion, the even subcarriers must be set to zero and hence half of the spectral efficiency is lost. On the other hand, DC-OFMD requires a large dc bias to make the signal positive and to avoid clipping distortions, but all subcarriers are used. We have also shown that bit loading and power allocation have little effect on DC-OFDM but can provide reduction up to 3 dB in the power penalty for ACO-OFDM.

The resolution required of the ADC/DAC is determined mainly by the constellation size. We have shown that ENOB values greater than 5 and 6 are necessary for 16-QAM and 64-QAM, respectively.

ACO-OFDM typically has 6 dB smaller power penalties and requires lower DAC/ADC resolution than DC-OFDM. However, owing to its poor spectral efficiency, ACO-OFDM requires sampling rates and DSP processing rates that are twice as high as DC-OFDM, which are prohibitively high for data center applications.

After ruling out the viability of ACO-OFDM, we extended the analysis of DC-OFDM to include CD and chirp, as well as shot and intensity noises. We showed that CD and chirp can be beneficial, due to the gain provided by the fiber intensity frequency response when transient chirp is dominant. However, as the fiber length increases, the phase-to-intensity conversion due to the combined effects of CD and chirp causes an additional penalty.

DC-OFDM can meet the required power budget under optical power constraints posed by eye safety. However, this technique offers only a small power margin, which is likely to make a system unreliable in practice. As an example, a 4-channel CWDM system with 5-dB link attenuation, using 16-QAM DC-OFDM with modulator bandwidth of 30 GHz and ENOB $= 5$, has a power margin of about 2.5 dB. As discussed in the companion paper [11], 4-PAM is the best-performing single-carrier scheme. It offers a power-margin of 6.5 dB for the same system discussed above. When modulator non-linarites are included, this margin drops to 4.9 dB.

This analysis has neglected the impact of modulator nonlinearities on multicarrier schemes. While these are not expected to alter the relative performance comparison between ACO-OFDM, DC-OFDM, and single-carrier schemes, they do affect the power penalty. Future work on multicarrier schemes should address the impact of these nonlinearities.

APPENDIX
OPTICAL POWER PENALTY IN AWGN CHANNEL

The BER of DC- and ACO-OFDM transmitted over an ideal optical AWGN channel with no bandwidth limitation and using ideal interpolation and antialiasing filter can calculated analytically as a function of the average optical power $\bar{P}$:

$$\text{BER} \approx$$

$$\begin{cases} \dfrac{4}{\log_2 M}\left(1 - \dfrac{1}{\sqrt{M}}\right)Q\left(\dfrac{R\bar{P}}{r}\sqrt{\dfrac{3}{M-1}\dfrac{\log_2 M}{N_0 R_b}}\right), & \text{DC} - \text{OFDM} \\[3mm] \dfrac{4}{\log_2 M}\left(1 - \dfrac{1}{\sqrt{M}}\right)Q\left(R\bar{P}\sqrt{\dfrac{3\pi}{M-1}\dfrac{\log_2 M}{2N_0 R_b}}\right), & \text{ACO} - \text{OFDM}. \end{cases}$$

$$(27)$$

For a given target BER we can normalize the required average optical power $\bar{P}_{req}$ by the required average optical power for NRZ-OOK $\bar{P}_{OOK,req}$ calculated in (17), and thus obtain the optical power penalty for each OFDM technique:

$$\frac{\bar{P}_{req}}{\bar{P}_{OOK,req}} = \begin{cases} r\sqrt{\dfrac{2(M-1)}{3\log_2 M}}, & \text{DC} - \text{OFDM} \\[3mm] \sqrt{\dfrac{4(M-1)}{3\pi\log_2 M}}, & \text{ACO} - \text{OFDM}. \end{cases}$$

$$(28)$$

Note that this expression was obtained by disregarding the multiplicative factors outside the Q-function in (27). This approximation makes (28) independent of the target BER.

ACKNOWLEDGMENT

REFERENCES

[1] C. Cole, "Beyond 100G client optics," *IEEE Commun. Mag.*, vol. 50, no. 2, pp. s58–s66, Feb. 2012.

[2] P. J. Winzer and J. Essiambre, "Advanced optical modulation formats," *Proc. IEEE*, vol. 94, no. 5, pp. 952–985, May 2006.

[3] A. Ghiasi and B. Welch, "Investigation of 100GbE based on PAM-4 and PAM-8," *IEEE 802.3bm Task Force*, Geneva, Switzerland, 2012.

[4] S. Bhoja, "Study of PAM modulation for 100GE over a single laser," *IEEE Next Generation 100G Optical Ethernet Study Group*, Newport Beach, CA, USA, 2012.

[5] C. Cole, I. Lyubomirsky, A. Ghiasi, and V. Telang, "Higher-order modulation for client optics," *IEEE Commun. Mag.*, vol. 51, no. 3, pp. 50–57, Mar. 2013.

[6] J. L. Wei, D. G. Cunningham, R. V. Penty, and I. H. White, "Study of 100 Gigabit Ethernet using carrierless amplitude/phase modulation and optical OFDM," *J. Lightw. Technol.*, vol. 31, no. 9, pp. 1367–1373, May 2013.

[7] M. I. Olmedo, T. Zuo, J. B. Jensen, Q. Zhong, X. Xu, S. Popov, and I. T. Monroy, "Multiband carrierless amplitude phase modulation for high capacity optical data links," *J. Lightw. Technol.*, vol. 32, no. 4, pp. 798–804, Feb. 2013.

[8] J. L. Wei, L. Geng, R. V. Penty, I. H. White, and D. G. Cunningham, "100 Gigabit Ethernet transmission enabled by carrierless amplitude and phase modulation using QAM receivers," in *Proc. Opt. Fiber Commun. Conf., Nat. Fiber Opt. Eng. Conf.*, 2013, pp. 1–3.

[9] W. A. Ling, I. Lyubomirsky, and O. Solgaard, "Digital quadrature amplitude modulation with optimized non-rectangular constellations for 100 Gb/s transmission by a directly-modulated laser: Abstract," *Opt. Exp.*, vol. 22, no. 9, pp. 10844–10857, 2014.

[10] J. D. Ingham, R. V. Penty, and I. H. White, "Orthogonal multipulse modulation in optical datacommunications," in *Proc. 15th Int. Conf. Transp. Opt. Netw.*, 2013, pp. 1–4.

[11] M. Sharif, J. K. Perin, and J. M. Kahn, "Modulation schemes for single-laser 100 Gbit/s Links: Single-carrier," *J. Lightw. Technol.*, vol. 33, no. 20, pp. 4268–4277, Oct. 2015.

[12] J. Armstrong and A. J. Lowery, "Power efficient optical OFDM," *Electron. Lett.*, vol. 42, no. 6, pp. 370–372, 2006.

[13] W. Kobayashi, T. Ito, T. Yamanaka, T. Fujisawa, Y. Shibata, T. Kurosaki, M. Kohtoku, T. Tadokoro, and H. Sanjoh, "50-Gb/s Direct modulation of a 1.3-um InGaAlAs-Based DFB laser with a ridge waveguide structure," *IEEE J. Sel. Topics Quantum Electron.*, vol. 19, no. 4, pp.1500908–1500908, Jul./Aug. 2013.

[14] Y. Yu, R. Lewen, S. Irmscher, U. Westergren, L. Thylen, U. Eriksson, and W. S. Lee, "80 Gb/s ETDM transmitter with a traveling-wave electroabsorption modulator," presented at the Optical Fiber Communication Conf., Nat. Fiber Optic Engineer Conf., Anaheim, CA, USA, 2005.

[15] O. Mitomi, S. Nojima, I. Kotaka, K. Wakita, K. Kawano, and M. Naganuma, "Chirping characteristic and frequency response of MQW optical intensity modulator," *J. Lightw. Technol.*, vol. 10, no. 1, pp. 71–77, Jan. 1992.

[16] G. Ghione, *Semiconductor Devices for High-Speed Optoelectronics*. Cambridge, U.K.: Cambridge Univ. Press, 2009, pp. 412–414.

[17] M. N. Ahmed, "Transimpedance amplifier (TIA) design for 400 Gb/s optical fiber communications," Master's thesis, Virginia Polytechnic Inst. State University, Blacksburg, VA, USA, 2013.

[18] *Optical Fibres, Cables and Systems*, International Telecommunications Union, Geneva, Switzerland, 2009, pp. 144–147.

[19] S. Bates, M. Gustlin, and J. Slavick, "FEC Options," *IEEE P802.3bj*, Newport Beach, CA, USA, Jan. 2011.

[20] J. M. Cioffi, *Lecture Notes EE379*, 2008, ch. 4, pp. 317–322.

[21] J. Campello, "Optimal discrete bit loading for multicarrier modulation systems," presented at the IEEE Int. Symp. Inform. Theory, Cambridge, MA, , 1998USA, 1998.

[22] J. J. Bussgang, "Crosscorrelation functions of amplitude-distorted Gaussian signals," *Res. Lab. Electron., Massachusetts Inst. Technol.*, Cambridge, MA, USA, Tech. Rep. 216, 1952, pp. 1–14.

[23] M. Möller, "High-speed electronic circuits for 100 Gb/s transport networks," presented at the Optical Fiber Communication Conf., Nat. Fiber Optic Engineers Conf., San Diego, CA, USA, 2010.

[24] T. Ellermeyer, R. Schmid, A. Bielik, J. Rupeter, and M. Möller, "DA and AD converters in SiGe technology: Speed and resolution for ultra high data rate applications," presented at the Eur. Conf. Optical Communication, Torino, Italy, 2010, p. Th.10.A.6.

[25] P. J. Winzer, "High-spectral-efficiency optical modulation formats," *J. Lightw. Technol.*, vol. 30, no. 24, pp. 3824–3835, Dec. 2012.

[26] H. V. Sorensen, M. Heideman, and C. S. Burrus, "On computing the split-radix FFT," *IEEE Trans. Acoust. Speech Signal Process.*, vol. ASSP-31, no. 1, pp. 152–156, Feb. 1986.

[27] K. Sato, S. Kuwahara, and Y. Miyamoto, "Chirp characteristics of 40-Gb/s directly Modulated distributed-feedback laser diodes," *J. Lightw. Technol.*, vol. 23, no. 11, pp. 3790–3797, Nov. 2005.

[28] F. Koyama and K. Iga, "Frequency chirping in external modulators," *J. Lightw. Technol.*, vol. 6, no. 1, pp. 87–93, Jan. 1988.

[29] B. Wedding, "Analysis of fibre transfer function and determination of receiver frequency response for dispersion supported transmission," *Electron. Lett.*, vol. 30, no. I, pp. 58–59, 1994.

[30] J. K. Perin, M. R. N. Ribeiro, and A. V. T. Cartaxo, "Polynomial-time complexity large-signal model for DML-Based OOFDM transmission systems," *J. Lightw. Technol.*, vol. 25, no. 24, pp. 2393–2396, Dec. 2013.

Authors' biographies not available at the time of publication.